RSC Advances

PAPER

View Article Online
View Journal | View Issue

Cite this: *RSC Adv.*, 2025, **15**, 28375

Low-energy room-temperature carbon dots for targeted sensing of MET inhibitor capmatinib

Mohamed N. Goda,[a] Laila S. Alqarni,[a] Hossieny Ibrahim,[b] Al-Montaser Bellah H. Ali[c] and Mohamed M. El-Wekil*[c]

Capmatinib (CMB) monitoring in biological fluids is critical for evaluating its pharmacokinetics, optimizing dosing, and minimizing toxicity. Accurate measurement is essential for ensuring therapeutic efficacy, enabling personalized treatment, and preventing adverse effects. Given the variability in patient metabolism and excretion, regular monitoring helps maintain CMB levels within the therapeutic range, improving treatment outcomes and minimizing the risk of drug resistance. This work presents an economical and energy-efficient strategy for preparing highly luminescent nitrogen-doped carbon dots (NCDs), employing 2,5-dihydroxy-1,4-benzoquinone alongside triethylenetetramine. The synthesized NCDs demonstrated excellent photostability and a high fluorescence quantum yield of 38.72%. Upon the addition of CMB, concentration-dependent fluorescence quenching was observed at 515 nm, which was attributed to the inner filter effect (IFE), with LOD of 3.6 nM. The NCDs exhibited high selectivity in detecting CMB, with minimal cross-reactivity from simultaneously present compounds. Recovery studies in real biological samples yielded rates between 97.4% and 105.3%, and RSDs were consistently below 4.11%. These results demonstrate the method's precision, reproducibility, and potential for reliable CMB detection in complex biological matrices.

Received 18th June 2025
Accepted 5th August 2025

DOI: 10.1039/d5ra04346h

rsc.li/rsc-advances

1. Introduction

Lung cancer is a common and serious disease, with non-small cell lung cancer (NSCLC) comprising about 85% of cases.[1] Capmatinib (CMB) is used to treat NSCLC with a MET exon 14 skipping mutation.[2] MET pathway dysregulation, driven by gene amplification or protein overexpression, contributes to cancer progression. CMB has demonstrated strong clinical efficacy in patients with MET mutations, despite common adverse effects like edema, nausea, and reduced appetite.[3] To ensure effective chemotherapy and minimize toxicity, precise monitoring of CMB concentrations in biological fluids is necessary. This highlights the need for a fast, reliable, and user-friendly electrochemical sensing platform. Several methods have been reported for the detection of CMB, primarily relying on chromatographic techniques such as HPLC-DAD, LC-MS/MS, UPLC-MS/MS, and electrochemical sensors.[4–8] While these methods offer high sensitivity and specificity, they often involve high operational costs, complex sample preparation steps, lengthy analysis times, and the need for sophisticated instrumentation and trained personnel. Electrochemical methods, though relatively low-cost, require electrode modification and careful surface regeneration to maintain sensitivity. A single fluorometric method has been reported, which enhances CMB's native fluorescence *via* surfactant addition;[7] however, its sensitivity remains limited (LOD 9 nM), and interference from plasma proteins can compromise accuracy.

In contrast, fluorometric techniques employing nanomaterial-based probes, such as carbon dots (CDs), present a promising alternative due to their simplicity, rapid analysis, low-cost synthesis, and high sensitivity.[9–11] To our knowledge, no method utilizing carbon dots for CMB detection has been previously reported. The method described in this study leverages NCDs, synthesized *via* a green, room-temperature Schiff base reaction, as a stable and selective fluorescent probe. Compared to chromatographic and electrochemical approaches, this strategy offers notable advantages in terms of cost-effectiveness, operational simplicity, energy efficiency, and suitability for rapid, sensitive detection in biological matrices.

Since their discovery in 2004 by Scrivens's group, CDs have attracted growing interest due to their low-cost synthesis, tunable fluorescence, water dispersibility, and biocompatibility. These features enable their use across diverse fields, including chemical sensing, drug delivery, photocatalysis, cancer therapy, optoelectronics, and cellular imaging.[12,13] Current CD synthesis strategies include hydrothermal/solvothermal,[14,15] microwave-assisted,[16,17] laser-based,[18,19] and chemical oxidation methods.[20,21] Hydrothermal and microwave methods dominate due to their versatility

[a]*Department of Chemistry, College of Science, Imam Mohammad Ibn Saud Islamic University (IMSIU), Riyadh 11623, Saudi Arabia*
[b]*Department of Chemistry, Faculty of Science, Assiut University, Assiut 71516, Egypt*
[c]*Department of Pharmaceutical Analytical Chemistry, Faculty of Pharmacy, Assiut University, Assiut, Egypt. E-mail: mohamed.elwakeel@pharm.aun.edu.eg; mohamed.mohamoud@ymail.com*

with raw materials,[22] but they often require high temperatures and specialized equipment, and result in complex purification steps due to by-products.[23] While chemical oxidation occurs at room temperature, it requires harsh reagents like concentrated acids, raising environmental and cost concerns. Therefore, developing a greener, low-energy synthesis approach remains a key goal.

Fluorescence quenching, a fundamental process in optical sensing, can occur *via* several mechanisms including dynamic quenching, static quenching, Förster Resonance Energy Transfer (FRET), and the Inner Filter Effect (IFE). Dynamic and static quenching involve direct molecular interactions between the fluorophore and quencher, either through collision in the excited state or ground–state complex formation, respectively. FRET relies on non-radiative energy transfer between donor and acceptor molecules in close proximity, requiring spectral overlap. In contrast, the IFE is a non-interactive optical attenuation process where the analyte absorbs either the excitation light (primary IFE) or the emitted fluorescence (secondary IFE), thereby diminishing the observed fluorescence intensity without altering the fluorophore's intrinsic photophysical properties or fluorescence lifetime.[24,25]

Leveraging the mild conditions of the Schiff base reaction between primary amines and carbonyl compounds,[26,27] a straightforward, single-step crosslinking process between 2,5-dihydroxy-1,4-benzoquinone and triethylenetetramine enabled the preparation of luminescent NCDs at room temperature. This facile method avoids the use of harsh chemicals, external energy input, or specialized equipment, supporting large-scale, green synthesis. The NCDs exhibit excitation-dependent photoluminescence, with peak emission at 515 nm (excitation at 405 nm). Due to their inner filter effect (IFE) with CMB, these NCDs serve as effective optical probes for CMB detection. No fluorometric method utilizing carbon dots has been reported in the literature for the determination of CMB. This highlights a clear research gap and underscores the novelty of employing carbon dot-based probes for CMB detection. Developing such a method could offer enhanced sensitivity, rapid analysis, and suitability for application in real samples.

2. Experimental

2.1. Materials and reagents

Capmatinib (CMB, 97.4%) and a range of potential interferents—ascorbic acid, uric acid, dopamine, glucose, tyrosine, phenylalanine, alanine, proline, glutathione, urea, arginine, leucine, glycine, all with purities ≥96.8%, were purchased from Sigma-Aldrich. Hydrochloric acid, rhodamine B, 2,5-dihydroxy-1,4-benzoquinone, triethylenetetramine, sodium hydroxide, acetonitrile, methanol, disodium hydrogen phosphate, and monosodium dihydrogen phosphate were analytical grade and obtained from Merck. All solutions were prepared using ultrapure Millipore water (18.2 MΩ cm).

2.2. Instruments, quantum yield calculation and real samples analysis

Details are included in the SI.

2.3. Synthesis of room temperature NCDs

A bottom-up synthesis of NCDs was performed at room temperature. 2,5-dihydroxy-1,4-benzoquinone (65 mg) and triethylenetetramine (1.54 mL) were dissolved in 20 mL of ultrapure water and stirred continuously for 14 h. The emergence of a dark brown solution indicated successful formation of NCDs. The product was filtered (0.22 μm) and dialyzed using a 3000 Da MWCO membrane against ultrapure water for 24 h. The purified NCDs were lyophilized and stored as a dry powder at 4 °C until use.

2.4. Fluorescence detection of CMB

A 250 μL aliquot of CMB solution (dissolved in methanol) at various concentrations was added to 300 μL of NCDs (12 mg mL^{-1}) and 450 μL of 0.01 M phosphate buffer (pH 7.0). After 2 min incubation at room temperature, fluorescence intensity was measured at 515 nm (excitation: 405 nm, slit width: 5 nm).

In order to investigate the selectivity of the system, CMB was replaced with diverse potential interfering substances, comprising metal ions, anions, various amino acids, and representative biomolecules such as dopamine, glucose, ascorbic acid, uric acid, glutathione, and urea.

3. Results and discussions

3.1. Characterization

NCDs emitting green fluorescence were synthesized *via* a mild Schiff base condensation of 2,5-dihydroxy-1,4-benzoquinone and triethylenetetramine at room temperature. This approach enabled *in situ* carbonization and nitrogen incorporation, with triethylenetetramine acting dually as a nitrogen source and cross-linking agent. The absence of post-functionalization steps and energy input makes the process efficient and scalable. TEM analysis (Fig. 1A) showed uniformly dispersed, spherical NCDs with diameters between 2.2 and 5.6 nm (average ~3.3 nm, Fig. 1B). High-resolution TEM images revealed lattice fringes of 0.22 nm, indicative of localized short-range ordering or partially graphitized domains within the amorphous carbon matrix.[28] The broad diffraction peak at $2\theta \approx 22.4°$ in the XRD pattern indicates an amorphous carbon structure with localized graphitic-like short-range ordering, consistent with partially disordered sp^2-hybridized domains.[29] The energy-dispersive X-ray (EDX) spectrum of the NCDs (Fig. 1D) confirms the presence of carbon (62.5%), nitrogen (23.7%), and oxygen (13.8%) as the primary elemental components, indicating successful doping and surface functionalization.

FTIR analysis (Fig. 2A) confirmed the presence of key functional groups on the surface of the NCDs. The broad band at 3272 cm^{-1} corresponds to O–H and N–H stretching vibrations, indicating hydroxyl and amine groups. The peak at 2887 cm^{-1} reflects aliphatic C–H stretching. A sharp absorption at 1692 cm^{-1} is attributed to C=O stretching of carbonyl groups. Bands at 1520 and 1390 cm^{-1} correspond to O–H bending and C=C stretching, respectively. The distinct peak at 770 cm^{-1} represents N–H out-of-plane bending, confirming successful nitrogen doping.

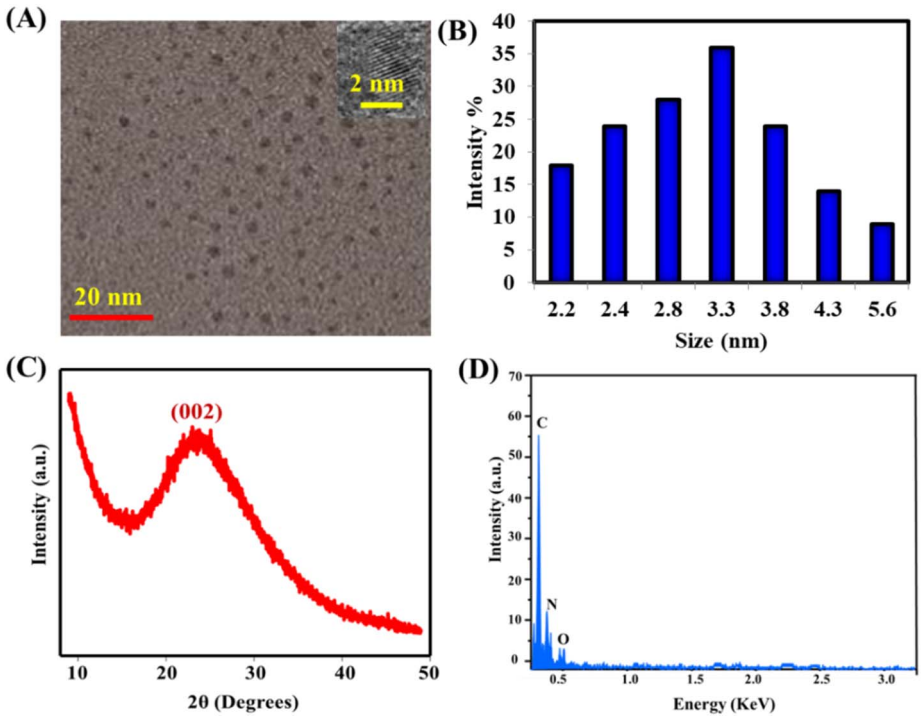

Fig. 1 (A) TEM image with inset HRTEM, (B) size distribution, (C) XRD pattern, and (D) EDX analysis of NCDs.

Raman spectroscopy (Fig. 2B) displayed prominent D (~1350 cm^{-1}) and G (~1580 cm^{-1}) bands, corresponding to disordered sp^3-hybridized carbon and graphitic sp^2-hybridized domains, respectively. The intensity ratio (I_D/I_G) of 1.54 indicates a high level of structural defects, consistent with a partially amorphous carbon framework. Emissive surface states from defects boost photoluminescence, and sp^2 domains preserve key properties, enabling NCDs for fluorescence sensing and bioimaging.[30]

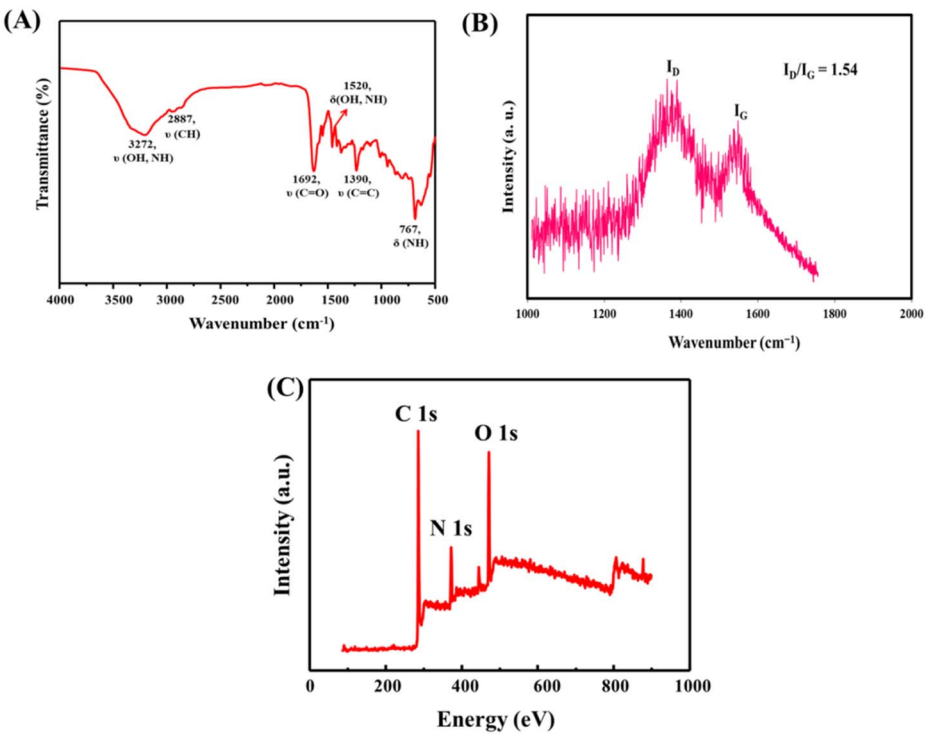

Fig. 2 FTIR (A), Raman spectrum (B), and XPS (C) survey of NCDs.

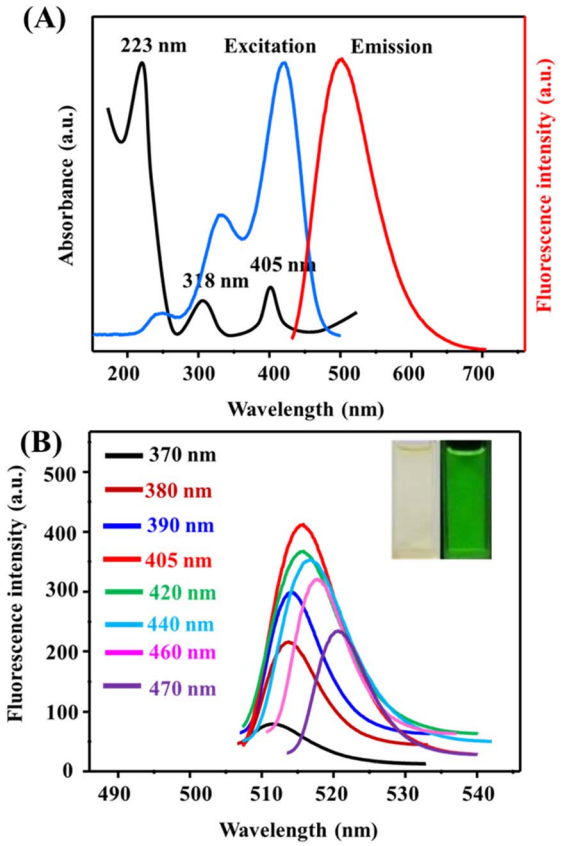

Fig. 3 (A) Absorption and fluorescence (excitation wavelength of 405 nm was applied, and emission spectra were collected from 450 nm to 710 nm spectra of NCDs) spectra. (B) Emission pattern of NCDs after excitation at different wavelengths (370–470 nm).

XPS analysis identified carbon, oxygen, and nitrogen on NCD surfaces, as shown in the wide-scan spectrum (Fig. 2C), as expected from the Schiff base condensation of 2,5-dihydroxy-1,4-benzoquinone and triethylenetetramine. The incorporation of nitrogen and oxygen atoms indicates the presence of functional groups such as amines, hydroxyls, and carbonyls, which contribute to the water solubility, biocompatibility, and fluorescence properties of the NCDs. Fig. S1 presents the deconvoluted peaks of C 1s, observed at 286.7 eV, 287.8 eV, and 289.9 eV, which correspond to C–C/C–H/C=C, C–O/C–N, and C=N functional groups, respectively.[31] Fig. S2 displays the deconvoluted peaks of N 1s, detected at 394.8 eV, 397.8 eV, and 401.7 eV, attributed to C–N/N–N, N–H, and C=N bonding environments, respectively.[32] Fig. S3 shows the deconvoluted peaks of O 1s, located at 532.6 eV and 536.3 eV, corresponding to C–O–C and C–O–H groups, respectively.[33]

UV-visible and fluorescence spectroscopy were used to assess the optical properties of NCDs. The UV-visible absorption spectrum revealed distinct peaks at 223 nm, 318 nm, and 405 nm, which can be attributed to π–π^*, n–π^* electronic transitions, and surface states within the NCDs' core, respectively,[34] as shown in Fig. 3A. In the fluorescence emission spectrum, a prominent emission peak was observed at 515 nm upon excitation at 405 nm, with excitation-dependent emissions spanning the range of 370–470 nm (Fig. 3B). The NCDs demonstrated stable green fluorescence at 515 nm (inset, Fig. 3B), accompanied by a quantum yield of 38.72%. This relatively high quantum yield can be attributed to the unique structural and electronic modifications induced by nitrogen doping. Nitrogen incorporation enhances the surface passivation of NCDs, facilitates efficient exciton recombination, and improves the π-conjugation of the carbon core. These effects mitigate non-radiative recombination processes, thereby enhancing the fluorescence emission.[35] The use of triethylenetetramine as a precursor and the mild synthesis conditions further preserve these desirable features, ensuring a high quantum yield. Fig. S4 shows the emission color coordinates were plotted on a CIE chromaticity diagram.

NCDs displayed stable fluorescence after 200 minutes of UV exposure (Fig. 4A), strong resistance to high NaCl concentrations (Fig. 4B), and consistent emission across pH 5–9 (Fig. 4C), with reduced intensity at extreme pH due to surface group protonation or deprotonation. Thermal stability was also confirmed, as the NCDs exhibited stable fluorescence from 25–90 °C (Fig. 4D). To assess the practical thermal stability, NCDs were dried, thermally treated at 60 °C, 80 °C, and 100 °C for 1 hour, and then redispersed in ultrapure water. The redispersed solutions exhibited >95% fluorescence recovery at 60–80 °C, with no visible aggregation. Even after exposure to 100 °C, the fluorescence retention remained above 90%, confirming the robust thermal resistance of the dried NCDs and their ability to recover functional properties upon redispersion. After 190 days of ambient storage, no signs of photobleaching or aggregation were observed (Fig. 4E). These findings highlight the NCDs' exceptional stability under various environmental conditions, including pH variations, high ionic strength, UV exposure, temperature fluctuations, and prolonged storage. Such stability enables their use in sustained analytical and biomedical tasks.

3.2. Optimization of conditions

As shown in Fig. 5, NCDs synthesis was optimized by varying 2,5-dihydroxy-1,4-benzoquinone (5–90 mg), triethylenetetramine (0.45–3.23 mL), and reaction time (5–25 hours). The optimal conditions—65 mg of 2,5-dihydroxy-1,4-benzoquinone, 1.54 mL of triethylenetetramine, and 14 hours of heating—yielded NCDs with high fluorescence intensity, narrow size distribution, and improved colloidal stability. These parameters enhanced the quantum yield by promoting efficient surface passivation and reducing particle aggregation during carbonization. The resulting NCDs exhibited consistent morphology, which supports their application in bioimaging and optical sensing platforms requiring stable and bright emission.

As shown in Fig. S5, NCD concentration (2–20 mg mL^{-1}), pH (5–9), and incubation time (0.5–5 min) were varied to optimize reaction conditions. The fluorescence response increased with concentration up to 12 mg mL^{-1}, beyond which the signal plateaued (Fig. S5A). This indicates saturation of binding sites on the target analyte, suggesting that 12 mg mL^{-1} ensures maximal surface interaction without inducing aggregation or

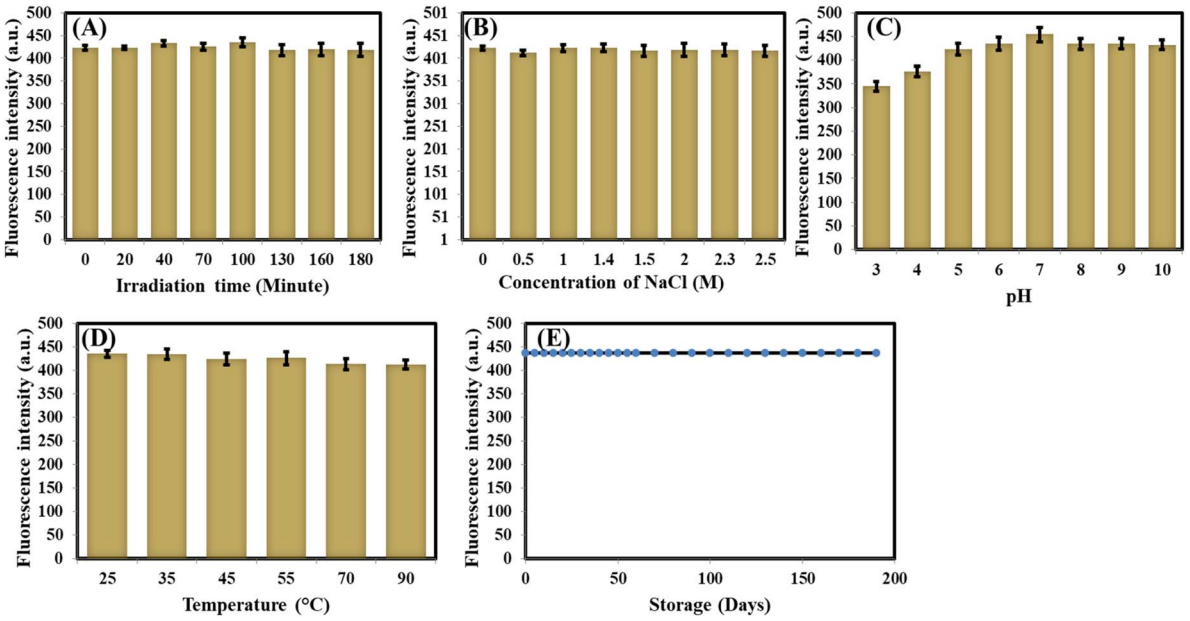

Fig. 4 Fluorescence responses of NCDs under different conditions including (A) irradiation time, (B) ionic strength, (C) pH, (D) temperature, and (E) storage days.

quenching effects. Optimal fluorescence was observed at pH 7.0 (Fig. S5B). Under these pH conditions, the amine functionalities of CMB ($pK_a \approx 5.4$) are partially protonated, while the carboxyl groups on the nitrogen-doped carbon dots ($pK_a \approx 4$–5) are deprotonated, establishing complementary charge interactions that drive electrostatic attraction. Simultaneously, both species retain active sites for hydrogen bonding, serving as donors and acceptors to strengthen molecular binding. The π–π stacking

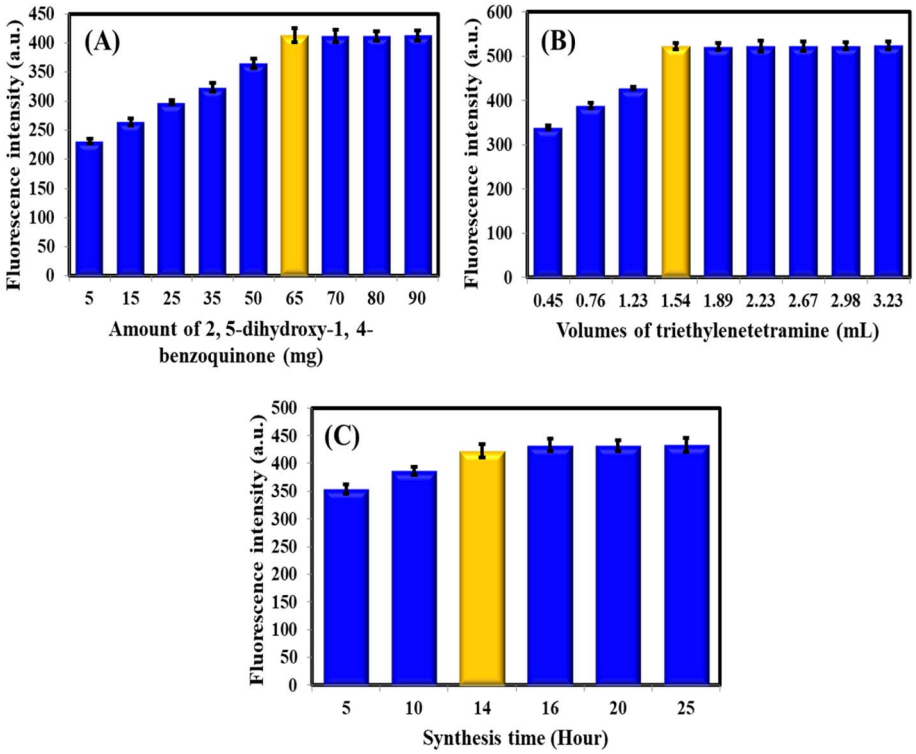

Fig. 5 Effect of (A) amount of 2,5-dihydroxy-1,4-benzoquinone (with triethylenetetramine volume fixed at 1.54 mL and reaction time at 14 hours), (B) volume of triethylenetetramine (with 65 mg for 2,5-dihydroxy-1,4-benzoquinone and reaction time at 14 hours), and (C) synthesis time (with 2,5-dihydroxy-1,4-benzoquinone amount fixed at 65 mg and triethylenetetramine at 1.54 mL) on the fluorescence intensity of NCDs.

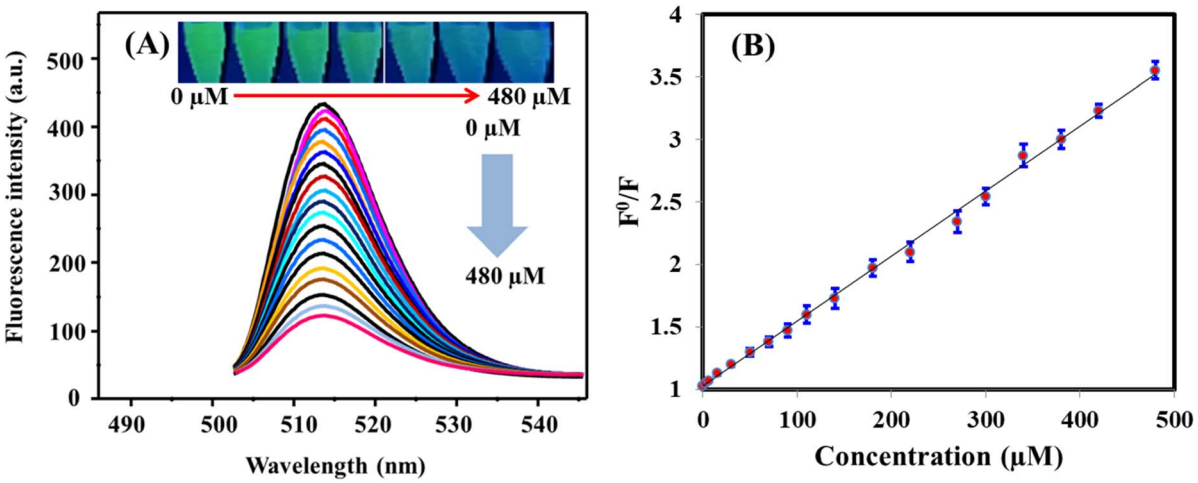

Fig. 6 (A) Fluorescence emission spectra of NCDs recorded after stepwise addition of CMB (0–480 μM). (B) Calibration plot correlating fluorescence responses with CMB concentration.

interactions between the aromatic rings of CMB and the graphitic planes of the NCDs further contribute to the overall stability of the formed complex. At lower or higher pH levels, altered protonation states weaken these interactions. The signal intensified rapidly and reached its maximum at 2 minutes (Fig. S5C). Prolonged incubation did not yield significant improvement, indicating fast kinetics and strong affinity under optimal conditions. Thus, 2 minutes was selected for all subsequent assays.

3.3. Quantitative estimation of CMB

The fluorescence response of NCDs to CMB was assessed by measuring emission intensity over concentrations ranging from 0 to 480 μM. Fig. 6A illustrates a gradual decrease in fluorescence intensity, with a notable 73.3% quenching observed at 480 μM CMB. A linear correlation was established between the fluorescence intensity ratio (F_0/F) and CMB concentration, described by the equation: $F_0/F = 1.024 + 0.005C_{CMB}$ where F_0 and F are the fluorescence intensities in the absence and presence of CMB, respectively. The detection limit for CMB was determined to be 0.0036 μM, based on a 3 : 1 signal-to-noise ratio (Fig. 6B). This method shows significant improvement in sensitivity compared to previous techniques (Table 1). For instance, a prior spectrofluorometric approach had a detection limit of 0.009 μM and was compromised by interference from plasma proteins.[7] This work pioneers a carbon-based nanomaterial method for CMB detection, with enhanced sensitivity and selectivity over prior techniques.

3.4. Mechanism

The fluorescence quenching pathway of NCDs by CMB was investigated through excitation and UV-Vis absorption spectra analysis. Fig. 7A shows notable spectral overlap, indicating energy transfer as a potential quenching mechanism. The fluorescence lifetime of NCDs remained almost unchanged in the presence of CMB, with a slight variation from 4.49 ns (without CMB) to 4.53 ns (with CMB) (Fig. 7B), indicating that the quenching is primarily due to the inner filter effect (IFE) rather than static or dynamic quenching mechanisms.[41] Zeta potential measurements revealed that the NCDs carry a net negative surface charge (−18.67 mV), while CMB carries a weak positive charge (+4.78 mV), suggesting the possibility of weak electrostatic attraction between the two species. However, given the low magnitude of the CMB's surface potential, electrostatic interactions are likely secondary to π–π stacking and hydrogen bonding in driving the NCD-CMB interaction (Fig. 7C). This electrostatic interaction further supports the conclusion that energy transfer between NCDs and CMB occurs primarily

Table 1 Quantitative parameters of the proposed and reported methods for CMB detection

Method	Linear range (μM)	LOD (μM)	Cost	Time	Complexity	Interference risk	Reference
HPLC-DAD	0.048–242.7	0.009	High	Slow	High	Moderate	7
HPLC-FLD	0.05–9.5	—	High	Slow	High	Moderate	36
UPLC-MS/MS	0.002–7.28	—	Very high	Slow	Very high	Low	37
Au@PAB/CNFs	0.01–20	0.005	Medium	Moderate	Moderate	Low to moderate	38
CeNPs@CNF-CF	—	0.05	Medium	Moderate	Moderate	Low to moderate	39
CeNPs@CNF-CF/PGRE	0.005–0.97	0.0014	Medium	Moderate	Moderate	Low to moderate	40
Spectrofluorometry	0.04–4.85	0.009	Low	Fast	Simple	High (plasma proteins)	7
	0–480	**0.0036**	**Low**	**Fast**	**Simple**	**Minimal**	**This work**

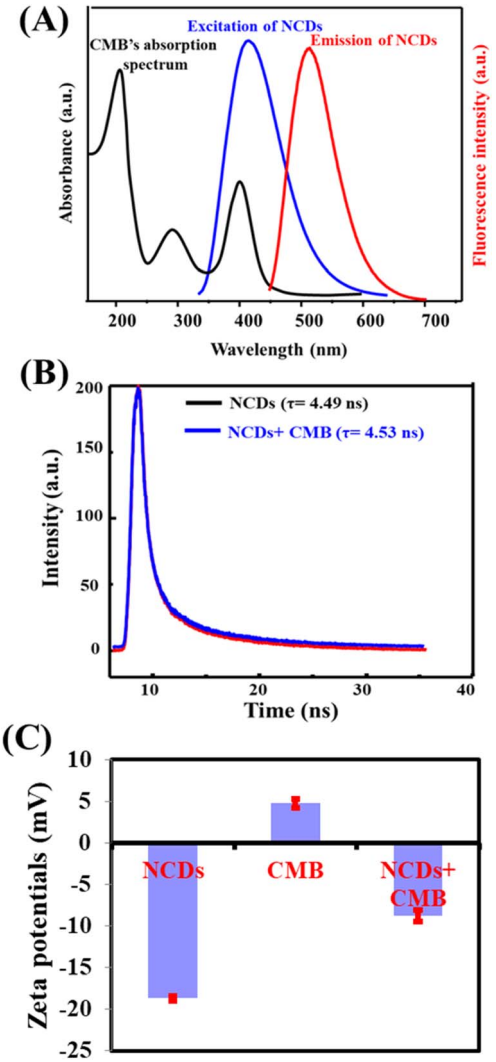

Fig. 7 (A) UV-Vis absorption of CMB with NCD excitation/emission spectra; (B) fluorescence lifetime comparison of NCDs and NCDs with CMB; (C) zeta potential measurements of NCDs, CMB, and their mixture.

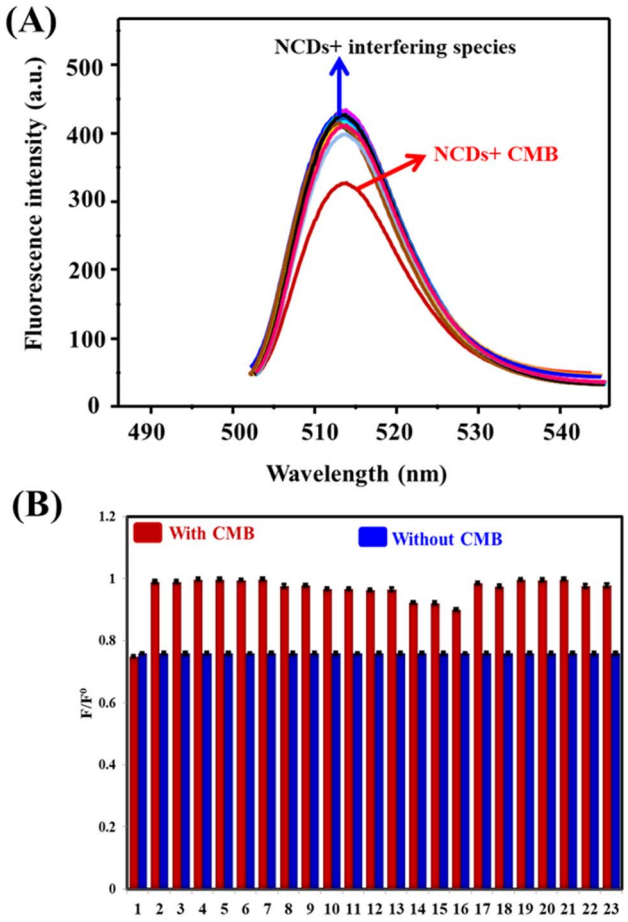

Fig. 8 (A) Fluorescence responses of NCDs upon addition 50 μM CMB and 60-fold interfering species. (B) Bar diagram comparing NCD fluorescence responses to CMB against various interfering species: 1. CMB, 2. Na^+, 3. K^+, 4. Mg^{2+}, 5. Ba^{2+}, 6. Ca^{2+}, 7. Zn^{2+}, 8. Cl^-, 9. SO_4^{2-}, 10. PO_4^{3-}, 11. tyrosine, 12. phenylalanine, 13. alanine, 14. arginine, 15. lysine, 16. histidine, 17. proline, 18. urea, 19. uric acid, 20. dopamine, 21. glutathione, 22. glucose, and 23. ascorbic acid.

through the IFE mechanism, with minimal perturbation to the fluorescence lifetime.[42]

3.5. Reproducibility and selectivity

Seven separate batches were prepared under identical conditions, and each was measured in triplicate to evaluate the method's reproducibility. The RSD of the readings did not exceed 2.87%, indicating excellent consistency and reproducibility across the samples. Quantum yields were determined using Rhodamine B as the reference standard, with values ranging from 39.78 to 37.65%, and an average of 38.72% (RSD = 0.87%). These results confirm the high reliability and reproducibility of the fluorometric probe for CMB detection, making it a robust tool for analytical applications.

To evaluate the selectivity of the NCDs for CMB, they were incubated with 50 μM CMB and a 60-fold excess of potential interferents. Significant fluorescence quenching was observed exclusively with CMB, while basic amino acids (lysine, arginine, and histidine) induced only minor quenching. This minimal quenching effect was attributed to electrostatic interactions, which were completely eliminated upon dilution. Further studies involving both CMB and interferents confirmed that the fluorescence quenching was predominantly due to CMB alone (Fig. 8). The pronounced selectivity observed in the figure can be primarily attributed to the inner filter effect (IFE), arising from the significant spectral overlap between the UV-Vis absorption bands of CMB and the excitation/emission wavelengths of the NCDs. Unlike other tested interferents, CMB effectively absorbs excitation/emission light, resulting in efficient fluorescence quenching *via* IFE. Additionally, CMB's planar aromatic structure, combined with nitrogen-containing heterocycles, facilitates stronger π–π stacking interactions with the graphitic-like domains of NCDs, as well as enhanced hydrophobic and hydrogen bonding interactions. These non-covalent interactions likely promote preferential adsorption of CMB onto the NCD surface, increasing its local concentration and further

Table 2 Determination of CMB using NCDs in urine and serum samples ($n = 5$)

		NCDs		
Samples	Added (μM)	Found (μM)	Recovery%	RSD%
Human urine	0.0	—	—	—
	5.0	5.08	101.6	3.67
	20.0	19.84	99.2	2.65
	50.0	52.67	105.3	1.98
Human serum	0.0	—	—	—
	5.0	4.87	97.4	4.11
	20.0	21.04	105.2	3.22
	50.0	49.76	99.5	2.87

enhancing IFE-based quenching. In contrast, the smaller, less conjugated, and more hydrophilic biomolecules tested lack sufficient spectral overlap and molecular affinity to induce significant quenching. This combination of spectral selectivity *via* IFE and structural complementarity underlies the high selectivity of the developed NCD probe for CMB detection.

While the current design offers minimal interference from coexisting substances, further optimization could enhance performance. In particular, adjusting the concentration of the NCD probe or fine-tuning the mixing ratio between the probe and sample could influence the degree of spectral overlap, optical pathlength, and surface interactions, thus modulating the sensitivity and selectivity of the system. By increasing the NCD concentration within limits that avoid self-quenching, or by optimizing the NCD-to-sample volume ratio, it may be possible to achieve improved analyte accessibility and signal-to-background ratio. These adjustments could be especially valuable when working with highly complex biological matrices or low-analyte-concentration environments. Future work may explore these parameters systematically to refine the probe's analytical performance.

3.6. Applications

To evaluate the potential of NCDs for CMB detection in biological samples, human serum and urine were spiked with CMB, and recovery was assessed using the standard addition method. The recovery rates ranged from 97.4 to 105.3% (Table 2), demonstrating high accuracy. The RSDs were consistently low, never exceeding 4.11%, which indicates excellent precision. These robust recovery rates, coupled with low RSDs, affirm the reliability and reproducibility of the NCD-based detection method. This makes it a highly suitable tool for sensitive and accurate CMB monitoring in complex biological matrices.

4. Conclusion (s)

A cost-effective, room-temperature synthetic approach was developed for producing NCDs, employing 2,5-dihydroxy-1,4-benzoquinone (5–90 mg) and triethylenetetramine as starting materials. These NCDs emitted stable green fluorescence, achieving a quantum yield of 38.72% (RSD = 0.87%). When applied for the detection of CMB, fluorescence quenching was observed, attributed to the IFE, with a remarkably low LOD of 0.0036 μM, highlighting their high analytical sensitivity. The NCDs showed strong selectivity with negligible biomolecular interference. Recovery tests in spiked serum and urine verified the method's suitability for real-sample analysis.

Ethical statement

The study received ethical approval from the Institutional Ethics Committee at the University of Assiut. Written informed consent was obtained from all participants prior to sample collection. All procedures involving human participants were conducted in accordance with the Declaration of Helsinki and applicable national regulations. Participant privacy and safety were safeguarded during collection, handling, analysis, storage, and disposal of biological samples.

Conflicts of interest

The authors declare no competing interests.

Data availability

Data will be available upon request from the corresponding authors.

Supplementary information is available. See DOI: **https://doi.org/10.1039/d5ra04346h**.

Acknowledgements

This work was supported and funded by the Deanship of Scientific Research at Imam Mohammad Ibn Saud Islamic University (IMSIU) (grant number IMSIU-DDRSP2501).

References

1 A. Upadhya, K. S. Yadav and A. Misra, *Expert Opin. Drug Delivery*, 2020, **18**, 73–102.
2 V. Moreno, R. Greil, J. Yachnin, M. Majem, M. Wermke, H. T. Arkenau, J. R. Basque, P. K. Nidamarthy, S. Kapoor, X. Cui and M. Giovanninim, *Clin. Ther.*, 2021, **4–6**, 1092–1111.
3 Y. L. Wu, L. Zhang, D. W. Kim, X. Liu, D. H. Lee, J. C. H. Yang, M. J. Ahn, J. F. Vansteenkiste, W. C. Su, E. Felip, V. Chia, S. Glaser, P. Pultar, S. Zhao, B. Peng, M. Akimov and D. S. W. Tan, *J. Clin. Oncol.*, 2018, **36**, 3101–3109.
4 U. Glaenzel, Y. Jin, R. Hansen, K. Schroer, G. Rahmanzadeh, U. Pfaar, V. J. J. Lier, H. Borell, A. Meissner, G. Camenisch and S. Zhao, *Drug Metab. Dispos.*, 2020, **48**, 873–885.
5 X. Fan, G. Yang, W. Cui, Q. Liu and Z. Zhang, *Biomed. Chromatogr.*, 2020, **34**, e4768.
6 C. Zhou, J. Tian, P. Lin, T. Liu, A. He, L. Fang and L. Sun, *Bioanalysis*, 2020, **12**, 285–293.
7 H. M. Ali, A. A. Essawy, I. H. Alsohaimi, A. Nayl, H. Ibrahim, A.-E.-N.-I. Essawy, M. Elmowafy and M. Gamal, *Microchem. J.*, 2022, **181**, 107838.

8 A. Zayed, S. A. A. Jaber, J. Al Hroot, S. Hawamdeh, N. M. Ayoub and N. A. Qinna, *Molecules*, 2022, **27**, 8582.
9 M. N. Goda, L. S. Alqarni, H. Ibrahim, A. B. H. Ali and M. M. El-Wekil, *Anal. Methods*, 2025, **17**, 5929–5938.
10 M. M. El-Wekil, Y. A. Bin Jardan, M. R. Elmasry and A. B. H. Ali, *Microchem. J.*, 2025, **212**, 113542.
11 Y. A. Bin Jardan, M. M. El-Wekil, M. R. Elmasry and A. B. H. Ali, *J. Photochem. Photobiol., A*, 2025, **468**, 116464.
12 B. Yao, H. Huang, Y. Liu and Z. Kang, Carbon dots: A small conundrum, *Trends Chem.*, 2019, **1**, 235–246.
13 Y. Hao, F. Ji, T. Li, M. Tian, X. Han and F. Chai, *Food Chem.*, 2024, **446**, 138843.
14 A. O. AlQarni, A. M. Mahmoud, R. Ali and M. M. El-Wekil, Colorimetric and fluorometric dual-mode determination of hypochlorite based on redox-mediated quenching, *RSC Adv.*, 2023, **13**, 32492–32501.
15 Y. Song, R. Xie, M. Tian, B. Mao and F. Chai, *J. Hazard. Mater.*, 2023, **475**, 131683.
16 S. A. Alkahtani, A. M. Mahmoud, Y. S. Alqahtani, A. B. H. Ali and M. M. El-Wekil, *Spectrochim. Acta, Part A*, 2023, **303**, 123252.
17 A. M. Mahmoud, S. S. Abu-Alrub, A. O. Alqarni, M. M. El-Wekil and A. B. H. Ali, *Microchem. J.*, 2023, **191**, 108929.
18 Y. M. Xian and K. Li, *Adv. Mater.*, 2022, **34**, 2201031.
19 L. Tang, L. Ai, Z. Q. Song, L. Z. Sui, J. K. Yu, X. Yang, H. Q. Song, B. W. Zhang, Y. S. Hu, Y. Q. Zhang, Y. Tian and S. Lu, *Adv. Funct. Mater.*, 2023, **33**, 2303363.
20 S. Dong, Y. L. Song, Y. Z. Fang, K. Zhu, K. Ye, Y. Y. Gao, J. Yan, G. L. Wang and D. A. X. Cao, *Carbon*, 2021, **178**, 1–9.
21 K. Ahmad, A. Pal, U. N. Pan, A. Chattopadhyay and A. Paul, *J. Mater. Chem. C*, 2018, **6**, 6691–6697.
22 Y. H. Cui, S. H. Xue, S. Y. Wang, X. Chen, S. J. Liu, Q. Ye, F. Zhou and W. M. Liu, *Carbon*, 2023, **205**, 373–382.
23 Z. F. Zhu, S. D. Wang, Y. J. Chang, D. B. Yu and Y. Jiang, *Carbon*, 2016, **105**, 416–423.
24 F. Zu, F. Yan, Z. Bai, J. Xu, Y. Wang, Y. Huang and X. Zhou, *Microchem. Acta*, 2017, **184**, 1899–1914.
25 Y. A. Bin Jardan, A. M. Mostafa, J. Barker, A. B. H. Ali and M. M. El-Wekil, *Anal. Methods*, 2025, **17**, 3007–3016.
26 L. Dordevic, F. Arcudi, M. Cacioppo and M. Prato, *Nat. Nanotechnol.*, 2022, **17**, 112–130.
27 Y. S. Li, X. X. Zhong, A. E. Rider, S. A. Furman and K. Ostrikov, *Green Chem.*, 2014, **16**, 2566–2570.
28 K. Bramhaiah, R. Bhuyan, S. Mandal, S. Kar, R. Prabhu, N. S. John, M. Gramlich, A. S. Urban and S. Bhattacharyya, *J. Phys. Chem. C*, 2021, **125**, 4299–4309.
29 V. M. Naik, S. V. Bhosalec and G. B. Kolekar, *Anal. Methods*, 2022, **14**, 877–891.
30 S. Rajendran, D. V. Ramanaiah, S. Kundu and S. K. Bhunia, *ACS Appl. Nano Mater.*, 2021, **4**, 10931–10942.
31 C. Y. Du, Y. Li, Y. Liu, N. Liu, Y. Cheng, Q. Shi, X. Liu, Z. Tao, Y. Guo and J. Zhang, *Front. Bioeng. Biotechnol.*, 2023, **11**, 1187632.
32 D. P. Huang, S. Xu, M. Zhang, W. Zhong, Z. Xiao and Y. Luo, *Mater. Chem. Phys.*, 2020, **240**, 122158.
33 E. B. Zheng, T. Liu, M. C. Paau, M. Wang, Y. Liu, L. Liu, C. Wu, J. Du, D. Xiao and M. M. Choi, *RSC Adv.*, 2015, **5**, 11667–11675.
34 D. Ozyurt, M. A. Kobaisi, R. K. Hocking and B. Fox, Properties, synthesis, and applications of carbon dots: a review, *Carbon Trends*, 2023, **12**, 100276.
35 A. M. Mahmoud, M. H. Mahnashi, S. A. Alkahtani and M. M. El-Wekil, *Inter. J. Biolg. Macromol.*, 2020, **165**(Part B), 2030–2037.
36 M. Yang, Y. Yan, E. Liu, X. Hu, H. Hao and J. Fan, *Optical Mater*, 2021, **112**, 110743.
37 X. Wang, Y. Liu, Q. Wang, T. Bu, X. Sun, P. Jia and L. Wang, *Spectrochim. Acta, Part A*, 2021, **244**, 118876.
38 A. Zayed, S. A. Jaber, J. Al Hroot, S. Hawamdeh, N. M. Ayoub and N. A. Qinna, *Molecules*, 2022, **27**, 8582.
39 M. W. Attwa, A. S. Abdelhameed, A. M. Alsibaee and A. A. Kadi, *Separations*, 2023, **10**, 247.
40 Y. S. Alqahtani, A. M. Mahmoud, B. A. Alyami, M. M. El-Wekil, H. M. Ali and H. Ibrahim, *Microchem. J.*, 2024, **201**, 110665.
41 A. Z. Alanazi, K. Alhazzani, M. M. El-Wekil, A. B. H. Ali, M. Darweesh and H. Ibrahim, *RSC Adv.*, 2024, **14**, 34448–34456.
42 A. Z. Alanazi, K. Alhazzani, M. M. El-Wekil, A. B. H. Ali, M. Darweesh and H. Ibrahim, *Talanta*, 2024, **279**, 126610.